Experimental Mechanics
DOI 10.1007/s11340-016-0174-x

Thermoelastic Stress Analysis of a Finite Orthotropic Composite Containing an Elliptical Hole

A. Alshaya[1] · **X. Shual**[2] · **R. Rowlands**[1]

Received: 2 December 2015 / Accepted: 18 May 2016

Abstract Individual stresses in a finite graphite/epoxy laminated composite containing an elliptical hole are determined from recorded load-induced thermal information. Equilibrium and compatibility conditions are satisfied using complex-variable formulation, conformal mapping and analytic continuation. Processing the measured thermal data with a stress function simultaneous smooths the measured data and evaluates the individual stress components, including on the edge of the hole. Reliability of experimental results is demonstrated by FEM and force equilibrium.

Keywords Thermoelastic stress analysis · Orthotropy · Composite materials · Elliptical holes · Complex variables

Introduction

Composite materials enjoy favorable specific strength and stiffness. Machine and structural members frequently contain holes or notches which produce stress concentrations. Purely analytical or theoretical stress analyses tend to be available for only simple situations involving infinite geometries, whereas many practical problems involve complicated, finite shapes. Moreover, and like numerical (FEM, FDM) approaches, analytical/theoretical analyses depend on reliable knowledge of the boundary conditions. The latter are often unknown in practice. Recognizing these situations, it is advantageous to be able to stress analyze experimentally members made of orthotropic composite materials. Candidate experimental approaches include moiré, speckle, holography, grids and digital image correlation. However, such displacement-based techniques necessitate differentiating the recorded data, something which can be unreliable. On the other hand, thermoelastic stress analysis (TSA) provides the stresses directly, without having to differentiate the measured information. Acknowledging the prevalence of elliptical cutouts in structures such as aerospace and transportation vehicles, and pressure vessels, this paper demonstrates the ability to determine the stresses in an elliptically perforated orthotropic composite member by TSA. The approach satisfies equilibrium and compatibility using a complex-variable formulation. Experimental reliability is demonstrated here by FEM and force equilibrium.

Thermoelastic stress analysis is a non-contacting, non-destructive experimental method for determining the full-field stresses in loaded members. The technique enables the stress analysis of actual structures in their operating environment with a sensitivity comparable to that of strain gages. No surface preparation is required other than perhaps a flat black paint to provide an enhanced and uniform emissivity. While many experimental techniques are labor-intensive and time consuming, commercially available hardware and software renders TSA efficient. By cyclically loading the structure to satisfy adiabatic reversible conditions, the stresses at a location are related to the stress-induced thermal information at that position. One records the TSA data with a sensitive infrared camera. For proportional loading of isotropic materials, the thermoelastic system signal, S^*, is related to the change in sum of the normal stresses, i.e.,

$$S^* = K\Delta(\sigma_{xx} + \sigma_{yy}) = K\Delta(p + q) = K\Delta(\sigma_{rr} + \sigma_{\theta\theta}) \quad (1)$$

✉ A. Alshaya
alshaya@wisc.edu

[1] University of Wisconsin-Madison, Madison, WI, USA

[2] Beijing Aeronautical Science & Technology Research Institute, Beijing, China

Published online: 01 June 2016

where K is an experimentally-determined thermomechanical coefficient, and p, q, σ_{rr}, $\sigma_{\theta\theta}$, σ_{xx} and σ_{yy} are the stresses in the principal, polar and Cartesian rectangular coordinates, respectively. Under orthotropy, S^*, is proportional to the following change in the linear combination of the normal stresses, σ_1 and σ_2, in the directions of material symmetry

$$S^* = \Delta(K_1\sigma_1 + K_2\sigma_2) \tag{2}$$

The orthotropic thermomechanical coefficients, K_1 and K_2, are traditionally determined experimentally. Although the recorded thermoelastic data at, and adjacent to, an edge are unreliable and raw thermoelastic information in composites is inherently noisy, the present technique overcomes these challenges by avoiding the use of recorded data on and near edges and processing the measured interior data with a stress function employing complex variables, mapping and analytic continuation. The resulting TSA-determined stresses are available on and in the neighborhood of the edge of the hole without knowing the distant geometry or boundary conditions.

References [1] through [7] are prior applications of TSA, including those with holes or notches, in orthotropic composite structures. Stanley and Chan [1] solved the restrictive case of a composite cylinder whose stresses are known from pressure-vessel theory, whereas Kageyama et al [2, 3] analyzed a composite containing a circular hole. Their method, while adequate for determining the stresses transverse to the fibers, seems to be otherwise unrealistic. Some of their results are also unreliable. Wong [4] proposed a non-adiabatic concept for stress analyzing orthotropic composites. The approach suffers from experimental scatter and fails to address the problem of unreliable edge information. Feng et al. [5] determined the stresses across the net section of a tensile composite strip containing a central circular hole. Although effective for this simple case, their approach is confined to along a line so the technique is not readily adaptable to general situations. Lin and Rowlands [6] evaluated the stresses in a notched laminate. Their analysis suffered from not having a systematic means of determining how many Airy coefficients to retain. Khaja, Samad and Rowlands [7, 8] recently obtained the individual stresses in elliptically-perforated aluminum plates, but the method is not applicable for orthotropy.

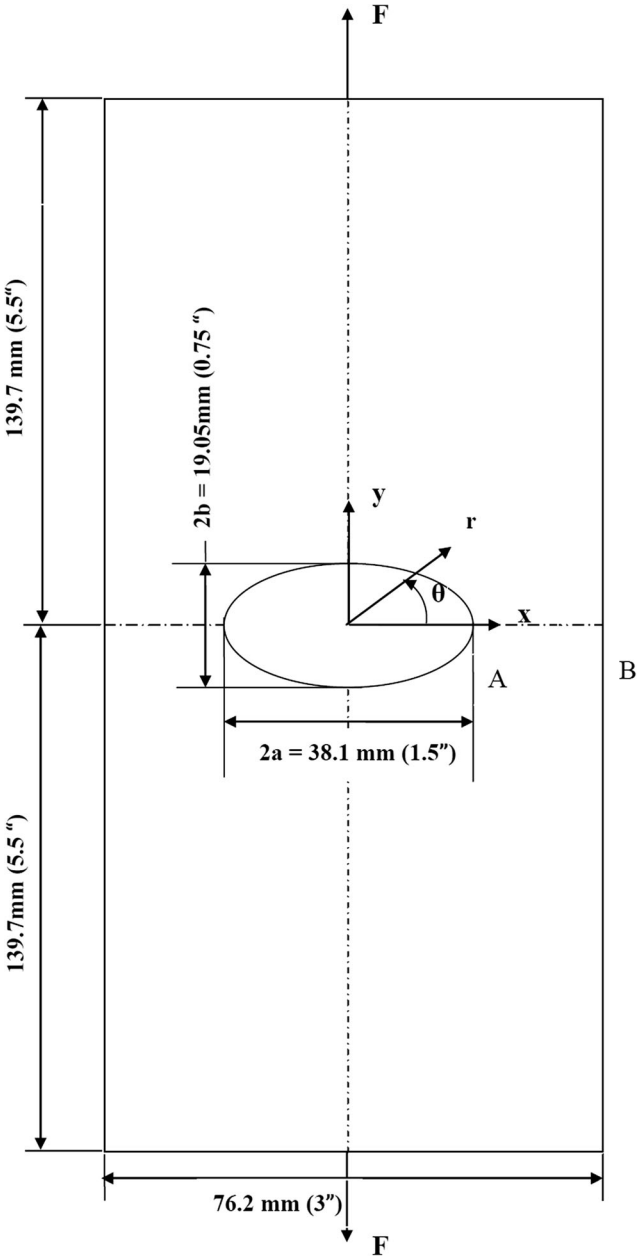

Fig. 1 Loaded finite Gr/E $[0_{13}/90_5/0_{13}]$ composite plate with central elliptical hole

Experimental Details

Geometry and Mechanical Properties

The developed hybrid-TSA approach is utilized to stress analyze a finite-width tensile $[0_{13}/90_5/0_{13}]$ graphite/epoxy orthotropic plate (from Kinetic Composites, Inc., Oceanside, CA) containing a central elliptical hole, Fig. 1. The 5.28 mm (0.21″) thick plate has an elliptical hole with semi-major axis $a = 19.1$ mm (0.75″) and semi-minor axis $b = 9.5$ mm (0.375″). The coordinate origin is at the center of the hole and the response is symmetric about both x- and y-axes. The laminate elastic properties were obtained from conducting uniaxial tensile tests in the strong/stiff (y-direction), weak/compliant (x-direction) and 45-degee orientations, [9]. These constitutive properties were obtained from two different sets of uniaxial tests (of E_{11}, E_{22}, E_{45} and ν_{12}). One set of strain-gaged coupons was loaded and unloaded once using hydraulic grips in a MTS testing machine, whereas the other set of gaged coupons was loaded and unloaded many times using the same grips and MTS machine. The values obtained from the first set of tests

are E_{11} = 107.9 GPa, E_{22}, = 30.4 GPa, G_{12} = 3.1 GPa and ν_{12} = 0.16. The averages of all the tests of the second set of tests are E_{11} = 101.0 GPa, E_{22}, = 25.6 GPa, G_{12} = 2.9 GPa and ν_{12} = 0.16. The averages of these two sets of values are listed in Table 1.

Plate Preparation

The plate was initially very lightly polished with 400 grit sand paper. TSA can be marginally conducted on graphite/graphite composites directly. However, we prefer applying a coating of Krylon Ultra-Flat black paint to provide an enhanced and uniform emissivity. Precaution was taken when sanding the faces of the plate to neither damage the fibers nor round-off the edge of the hole which could further erode the quality of the thermal information close to the edge of the hole.

Loading

The plate was subjected to a cyclically varying sinusoidally load in a 20 kips capacity MTS hydraulic testing machine with a mean value of 7.1 kN (1600 lbs.), maximum value of 10.7 kN (2400 lbs.) and a minimum value of 3.6 kN (800 lbs.) at a rate of 20 Hz. Our experience indicates this is a suitable frequency to use with perforated graphite/epoxy composites. Phase information was also monitored to ensure that adiabatic conditions were maintained. The corresponding load-induced TSA data were recorded using a liquid-nitrogen cooled TSA Delta Therm model DT1410 system having a sensor array of 256 horizontal by 256 vertical pixels (Stress Photonics, Madison, WI).

TSA Recording

The thermoelastic system signal, S^*, was recorded by the data acquisition system which is equipped with Delta Vision Software, Fig. 2(a). TSA images were captured and averaged over two minutes durations, and then exported to Excel while converting each pixel into a data point, i.e., 256 by 256 matrix. Pixel size is 0.35 mm (0.014 inch). Since TSA data typically are unreliable on and near an edge, no recorded TSA information was used within six pixel positions (0.1 a = 2 mm) of the edge of the hole.

Table 1 Laminate elastic properties*

Elastic Modulus, E_{11}	104.4 GPa = 15.0 × 10^6 psi
Elastic Modulus, E_{22}	28.0 GPa = 4.0 × 10^6 psi
Shear Modulus, G_{12}	3.0 GPa = 0.43 × 10^6 psi
Poisson's ratio, ν_{12}	0.16

*The 1- and 2-orientations are directions of laminate material symmetry. They are in the longitudinal/vertical and transverse/horizontal directions, respectively, Fig. 1

TSA Calibration

The thermoelastic coefficients K_1 and K_2 were evaluated from uniaxial tensile coupons loaded in the strong/stiff (vertical, y -direction) and weak/compliant (horizontal, x -direction) laminate orientations of the orthotropic $[0_{13}/90_5/0_{13}]$ composite plate. These coupons were painted and tested at 20 Hz on the same day as the elliptically-perforated plate. From equation (2), the values of the thermomechanical coefficients were determined to be K_1 = 1.8 mU/MPa (12.38 U/psi) and K_2 = 14.7 mU/MPa (101.25 U/psi). The unit U is used to signify the raw TSA output, in uncalibrated signal units.

Data Processing

Figure 2(a) is a contour plot of the raw measured thermoelastic data throughout a rectangular region containing the hole in the orthotropic composite ($E_{11}/E_{22} \sim 4$). The individual stresses throughout the region containing the elliptical hole were determined from such thermoelastic data. Since the plate behavior is symmetrical about the vertical y - and horizontal x -axes, the recorded thermoelastic data, S^*, of Fig. 2(a) were averaged throughout the four quadrants. The resulting S^* information is plotted in the first quadrant in Fig. 2(b). Due to unreliability, the recorded data along and near the edge of the hole were not used. Only the thermal information within the region covered by 1.1 a (21 mm) and 1.1 b (10.5 mm) to 1.85 a (35.2 mm) and 1.85 b (17.6 mm) was considered, as indicated by the source locations of the 2558 values of S^* shown in Fig. 3. The region of Fig. 3 will be denoted as R^*. Like most experimental data, the recorded S^* values include some noise which necessitates collecting more measured input values than the number of unknown Airy coefficients, i.e., the number of equations, P, will exceed the number of real coefficients, $2N$. The resulting overdetermined system of equations with which to evaluate the Airy coefficients was solved using least-squares. The subsequent analysis demonstrates that the described approach is able to evaluate stresses reliably at the edge of the elliptical hole without using any thermoelastic data on, or very near, the edge. Recognizing the most important stresses occur on or near the edge of the hole, only a 'ring shaped' segment, Figs. 2(b) and 3, rather than the entire quadrant, Fig. 2(a), was considered.

Relevant Equations

Basic Equations

The method behind determining the state of stress at and near a geometry discontinuity lies in coupling the Airy stress function with the measured thermoelastic data, and hence the term *hybrid*. For plane problems having rectilinear orthotropy and

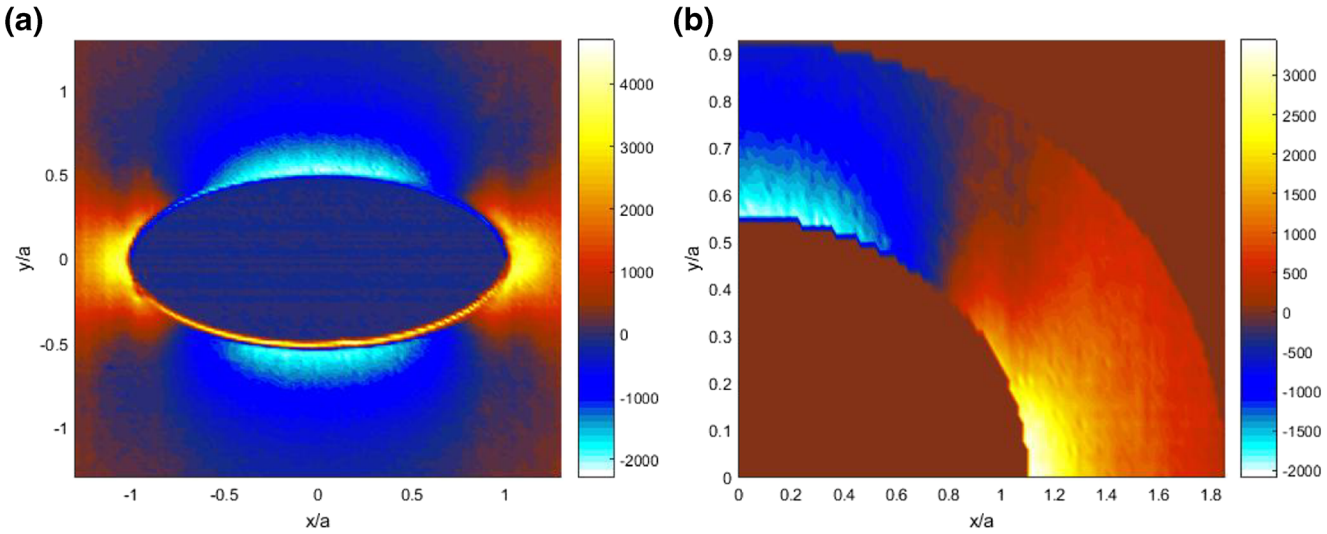

Fig. 2 (**a**) TSA image, S^*, of perforated orthotropic plate loaded; (**b**) averaged thermoelastic data, S^*, throughout the four quadrants at a range of 7.12 kN (1600 lbs.)

no body forces, the Airy stress function, F, satisfying $\nabla^4 F = 0$, can be expressed as a summation of two arbitrary analytical functions, $F_1(z_1)$ and $F_2(z_2)$, in terms of the complex variables, z_1 and z_2, as [10]

$$F = 2Re[F_1(z_1) + F_2(z_2)] \tag{3}$$

such that $z_j = x + \mu_j y$ for $j = 1, 2$ and Re denotes the 'real part' of a complex number. The complex material properties μ_1 and μ_2 are two distinct roots of the following characteristic equation associated with the compatibility equation

$$a_{11}\mu^4 + (2a_{12} + a_{66})\mu^2 + a_{22} = 0 \tag{4}$$

where a_{ij} are the elastic compliances occurring in the generalized Hooke's law. With $a_{11} = 1/E_{11}$, $a_{12} = -\nu_{12}/E_{11}$, $a_{22} = 1/E_{22}$, and $a_{66} = 1/G_{12}$, the characteristic equation becomes

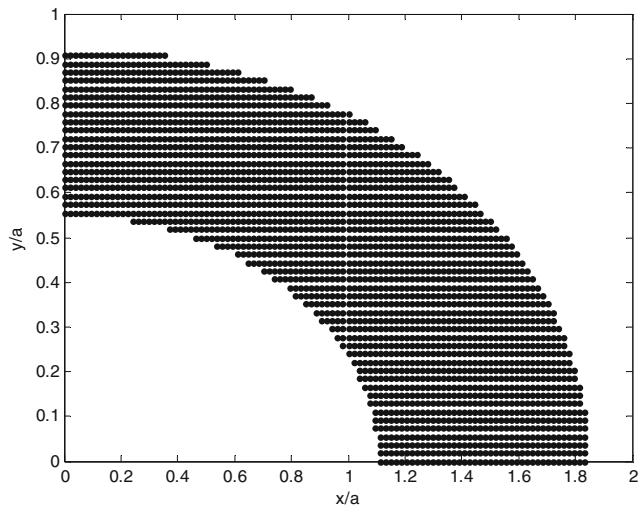

Fig. 3 Source locations of employed S^* data (P = 2558 data points)

$$\mu^4 + \left(\frac{E_{11}}{G_{12}} - 2\nu_{12}\right)\mu^2 + \frac{E_{11}}{E_{22}} = 0 \tag{5}$$

The 1- and 2-orientations are the directions of laminate material symmetry, and are in the longitudinal/vertical and transverse/horizontal directions, respectively, Fig. 1. The roots of equations (5) are complex, i.e., $\mu_1 = \alpha + i\beta$, $\mu_2 = \gamma + i\delta$, $\mu_3 = \overline{\mu}_1$, and $\mu_4 = \overline{\mu}_2$. The stresses in rectangular coordinates (x, y) of the physical $z(=x+iy)$ plane can now be expressed in terms of the stress function. By introducing the new stress functions

$$\Phi(z_1) = \frac{dF_1(z_1)}{dz_1}, \quad \text{and} \quad \Psi(z_2) = \frac{dF_2(z_2)}{dz_2} \tag{6}$$

the stresses can be written as

$$\sigma_x = 2Re\left[\mu_1^2\Phi'(z_1) + \mu_2^2\Psi'(z_2)\right] \tag{7}$$

$$\sigma_y = 2Re\left[\Phi'(z_1) + \Psi'(z_2)\right] \tag{8}$$

$$\tau_{xy} = -2Re\left[\mu_1\Phi'(z_1) + \mu_2\Psi'(z_2)\right] \tag{9}$$

where primes denote differentiation with respect to the argument. Plane problems of elasticity classically involve determining the stress functions, $\Phi(z_1)$ and $\Psi(z_2)$, throughout a component and subject to the boundary conditions around its entire edge. For a region of a component adjacent to a traction free-edge, Φ and Ψ can be related to each other by the conformal mapping and analytic continuation techniques. The stresses can therefore be expressed in terms of the single stress function, Φ. Moreover, Φ will be represented by a truncated power-series expansion whose unknown complex coefficients can all be evaluated from experimental measured data.

Once Φ and Ψ are fully evaluated, the individual stresses are available from equations (7) through (9). For a significantly large region, it may be necessary to satisfy other boundary conditions at discrete locations.

Conformal Mapping

Conformal mapping is introduced to simplify the plane problem by mapping the region R_z of a complicated physical $z=x+iy$ plane of a loaded component into a region R_ζ of a simpler shape of the $\zeta=\xi+i\eta$ plane, the latter being a half plane or unit circle. This mapping function preserves angles and maps a section of the real axis of the ζ plane, Γ_ζ, into the traction-free boundary condition, Γ, of the physical region, R_z, of the loaded component. The new coordinate system (and resulting geometry) is usually chosen to aid in solving the equations and the obtained solution from this simplified domain can then be mapped back to the original physical geometry for a valid solution. Assume that a mapping function of the form

$$z = \omega(\zeta) \tag{10}$$

exists and which maps R_ζ of the simpler plane into R_z of the more complicated physical plane. For orthotropy, auxiliary planes and their induced mapping functions are defined in terms of $\zeta_j=\xi+\mu_j\eta$ so by substituting $z_j=x+\mu_j y$ into equation (10) one obtains

$$z_j = \omega_j(\zeta_j), \quad j = 1,2 \tag{11}$$

The induced conformal mapping functions are therefore one-to-one and invertible. The stress functions Φ and Ψ can now be expressed as analytic functions of ζ_1 and ζ_2, respectively,

$$\Phi(z_1) = \Phi[\omega_1(\zeta_1)] \equiv \Phi(\zeta_1) \tag{12}$$

$$\Psi(z_2) = \Psi[\omega_2(\zeta_2)] \equiv \Psi(\zeta_2) \tag{13}$$

The derivatives of these stress functions with respect to each argument are

$$\Phi'(z_1) = \Phi'(\zeta_1)\frac{d\zeta_1}{dz_1} = \frac{\Phi'(\zeta_1)}{\omega_1'(\zeta_1)} \tag{14}$$

$$\Psi'(z_2) = \frac{\Psi'(\zeta_2)}{\omega_2'(\zeta_2)} \tag{15}$$

The analyticity of the mapping functions satisfies the equilibrium and compatibility equations throughout region R_z of the physical plane. Using the concept of analytic continuation, the stress functions for a region R_z adjacent to a traction-free boundary of an orthotropic material are related by [11, 12]

$$\Psi(\zeta_2) = B\overline{\Phi\left(\overline{\zeta_2}\right)} + C\Phi(\zeta_2) \tag{16}$$

where constants B and C are the following complex material properties

$$B = \frac{\overline{\mu}_2-\overline{\mu}_1}{\mu_2-\overline{\mu}_2}, \quad C = \frac{\overline{\mu}_2-\mu_1}{\mu_2-\overline{\mu}_2} \tag{17}$$

Equation (16) enables the elastic state of the structure to be expressed in terms of a single stress function, $\Phi(\zeta_1)$, the latter which can be represented by a truncated either Taylor series or Laurent series. Mapping the boundary of the hole in the physical z -plane to the real axis of the ζ -plane uses a truncated Taylor series expansions whereas mappings the boundary of the physical plane to the unit circle in the ζ -plane employs a Laurent series. The finite Taylor series expansion of the stress function is [13]

$$\Phi(\zeta_1) = \sum_{j=0}^{N} A_j(\zeta_1-\zeta_0)^j \tag{18}$$

whereas the stress function expressed as Laurent series expansion is [13]

$$\Phi(\zeta_1) = \sum_{\substack{j=-N,\ldots \\ j\neq 0}}^{N} A_j\zeta_1^j \tag{19}$$

and $A_j=a_j+ib_j$ are the unknown complex coefficients, ζ_0 is some point on the traction-free boundary and the summation in Laurent expansion involves only odd values of j. Substituting equation (18) or (19) into equation (16) yields

$$\Psi(\zeta_2) = \sum_{j=0}^{N}\left(\overline{A}_jB + A_jC\right)(\zeta_2-\zeta_0)^j \tag{20}$$

when using a Taylor series while for a Laurent expansion it is

$$\Psi(\zeta_2) = \sum_{\substack{j=-N,-N+2,\ldots \\ j\neq 0}}^{N}\left(\overline{A}_jB\zeta_2^{-j} + A_jC\zeta_2^{j}\right) \tag{21}$$

$\bar{A}_j$ is the complex conjugate of A_j. At least for a finite simply-connected region R_ζ, $\Phi(\zeta_1)$ is a single-valued analytic function.

Upon combining equations (6) through (20), one obtains the following expressions for the stress if using a Taylor series,

$$\sigma_{xx} = 2\sum_{j=1}^{N} Re\left\{\left[\frac{j\mu_1^2}{\omega_1'(\zeta_1)}(\zeta_1-\zeta_0)^{j-1} + \frac{j\mu_2^2 C}{\omega_2'(\zeta_2)}(\zeta_2-\zeta_0)^{j-1}\right]A_j + \left[\frac{j\mu_2^2 B}{\omega_2'(\zeta_2)}(\zeta_2-\zeta_0)^{j-1}\right]\overline{A}_j\right\} \tag{22}$$

$$\sigma_{yy} = 2\sum_{j=1}^{N} Re\left\{\left[\frac{j}{\omega_1'(\zeta_1)}(\zeta_1-\zeta_0)^{j-1} + \frac{jC}{\omega_2'(\zeta_2)}(\zeta_2-\zeta_0)^{j-1}\right]A_j + \left[\frac{jB}{\omega_2'(\zeta_2)}(\zeta_2-\zeta_0)^{j-1}\right]\overline{A}_j\right\} \tag{23}$$

$$\sigma_{xy} = -2\sum_{j=1}^{N} Re\left\{\left[\frac{j\mu_1}{\omega_1'(\zeta_1)}(\zeta_1-\zeta_0)^{j-1} + \frac{j\mu_2 C}{\omega_2'(\zeta_2)}(\zeta_2-\zeta_0)^{j-1}\right]A_j + \left[\frac{j\mu_2 B}{\omega_2'(\zeta_2)}(\zeta_2-\zeta_0)^{j-1}\right]\overline{A}_j\right\} \tag{24))}$$

Upon combining equations (6) through (19) and (21) when using a Laurent series, the individual stresses can be expressed as

$$\sigma_{xx} = 2\sum_{\substack{j=-N,-N+2,\ldots \\ j\neq 0}}^{N} Re\left\{j\left[\frac{\mu_1^2{\zeta_1}^{j-1}}{\omega_1'(\zeta_1)} + \frac{C\mu_2^2{\zeta_2}^{j-1}}{\omega_2'(\zeta_2)}\right]A_j - j\mu_2^2 B\left[\frac{{\zeta_2}^{-j-1}}{\omega_2'(\zeta_2)}\right]\overline{A}_j\right\} \tag{25}$$

$$\sigma_{yy} = 2\sum_{\substack{j=-N,-N+2,\ldots \\ j\neq 0}}^{N} Re\left\{j\left[\frac{{\zeta_1}^{j-1}}{\omega_1'(\zeta_1)} + \frac{C{\zeta_2}^{j-1}}{\omega_2'(\zeta_2)}\right]A_j - jB\left[\frac{{\zeta_2}^{-j-1}}{\omega_2'(\zeta_2)}\right]\overline{A}_j\right\} \tag{26}$$

$$\sigma_{xy} = -2\sum_{\substack{j=-N,-N+2,\ldots \\ j\neq 0}}^{N} Re\left\{j\left[\frac{\mu_1{\zeta_1}^{j-1}}{\omega_1'(\zeta_1)} + \frac{C\mu_2{\zeta_2}^{j-1}}{\omega_2'(\zeta_2)}\right]A_j - j\mu_2 B\left[\frac{{\zeta_2}^{-j-1}}{\omega_2'(\zeta_2)}\right]\overline{A}_j\right\} \tag{27}$$

The only unknowns in these expressions for the stresses are the complex coefficients, A_j. The latter can be determined from measured thermoelastic data. Choosing the $y-$ axis parallel to the strongest, stiff orientation of the composite, Fig. 1, i.e., 1-direction of an orthotropic composite material, and introducing the Taylor series according to equation (18), the TSA signal S^* can be expressed as

$$\begin{aligned} S^* &= K_1\sigma_{yy} + K_2\sigma_{xx} \\ &= 2\sum_{j=1}^{N} Re\left\{\left[\frac{j\left(K_1+K_2\mu_1^2\right)}{\omega_1'(\zeta_1)}(\zeta_1-\zeta_0)^{j-1} + \frac{j\left(K_1+K_2\mu_2^2\right)C}{\omega_2'(\zeta_2)}(\zeta_2-\zeta_0)^{j-1}\right]A_j + \left[\frac{j\left(K_1+K_2\mu_2^2\right)B}{\omega_2'(\zeta_2)}(\zeta_2-\zeta_0)^{j-1}\right]\overline{A}_j\right\} \end{aligned} \tag{28}$$

Upon introducing the Laurent series according to equation (19), the thermoelastic data S^* becomes

$$S^* = K_1\sigma_{yy} + K_2\sigma_{xx} = 2\sum_{\substack{j=-N,-N+2,\ldots \\ j\neq 0}}^{N} Re\left\{\left[\frac{j\left(K_1+K_2\mu_1^2\right)}{\omega_1'(\zeta_1)}\zeta_1{}^{j-1} + \frac{j\left(K_1+K_2\mu_2^2\right)C}{\omega_2'(\zeta_2)}\zeta_2{}^{j-1}\right]A_j - \left[\frac{j\left(K_1+K_2\mu_2^2\right)B}{\omega_2'(\zeta_2)}\zeta_2{}^{-j-1}\right]\overline{A}_j\right\} \tag{29}$$

The thermoelastic data, S^*, at P different locations are chosen to be inside the region R^*, Fig. 3. Equations (28) and (29) each forms a system of simultaneous linear equations, $[M]_{P\times 2N}\{c\}_{2N\times 1} = \{S^*\}_{P\times 1}$, where matrix $[M]$ consists of analytical expression of S^*, vector $\{c\}_{2N\times 1} = \{a_1, b_1, a_2, b_2, \ldots, a_N, b_N\}$ has $2N$ unknown real coefficients (a_j and b_j) and vector $\{S^*\}_{P\times 1}$ has P equations such that $P \gg 2N$. The best values of the coefficients, A_j, in a least-squares numerical sense, can be determined from measured values of S^*. The variables $\zeta_j = \xi + \mu_j\eta$, in equations (28) and (29) are related to the physical locations $z = x + iy$ through the inverse mapping function $z_j = \omega_j(\zeta_j)$. The individual stresses are then known throughout the region R_z, including on the traction-free edge Γ from equations (22) through (24) if using the Taylor expansion or from equations (25) through (27) if using the Laurent expansion.

Stresses in Polar and Elliptical Coordinates

The polar components of stresses are evaluated by converting the Cartesian stresses using standard transformation matrix

$$\begin{bmatrix}\sigma_{rr}\\ \sigma_{\theta\theta}\\ \sigma_{r\theta}\end{bmatrix} = \begin{bmatrix}\cos^2\theta & \sin^2\theta & 2\sin\theta\cos\theta\\ \sin^2\theta & \cos^2\theta & -2\sin\theta\cos\theta\\ -\sin\theta\cos\theta & \sin\theta\cos\theta & \cos^2\theta - \sin^2\theta\end{bmatrix}\begin{bmatrix}\sigma_{xx}\\ \sigma_{yy}\\ \sigma_{xy}\end{bmatrix} \tag{30}$$

The stresses in elliptical coordinates, where n is the normal to the edge of the elliptical hole and t is the tangential to the edge of the hole, can then be obtained from equation (31)

$$\begin{bmatrix}\sigma_{nn}\\ \sigma_{tt}\\ \sigma_{nt}\end{bmatrix} = \begin{bmatrix}\cos^2\psi & \sin^2\psi & 2\sin\psi\cos\psi\\ \sin^2\psi & \cos^2\psi & -2\sin\psi\cos\psi\\ -\sin\psi\cos\psi & \sin\psi\cos\psi & \cos^2\psi - \sin^2\psi\end{bmatrix}\begin{bmatrix}\sigma_{rr}\\ \sigma_{\theta\theta}\\ \sigma_{r\theta}\end{bmatrix} \tag{31}$$

with $\psi = \alpha - \theta$, as shown in Fig. 4. Using elliptical geometry, the normal angle, α, is evaluated from

$$\alpha = \tan^{-1}\left(\frac{a^2\tan\theta}{b^2}\right) \tag{32}$$

From equation (31), the components of stress σ_{tt}, tangential to the edge of the elliptical hole is given by

$$\sigma_{tt} = \sin^2\psi\sigma_{rr} + \cos^2\psi\sigma_{\theta\theta} - 2\sin\psi\cos\psi\sigma_{r\theta} \tag{33}$$

Mapping Formulations for an Elliptical Shape [6]

The objective here is to apply the approach to a region R_z adjacent to a traction-free boundary of a physical member provided an appropriate mapping function is available to map the region R_ζ into region R_z, where Γ_ζ, a section of the real axis in the ζ -plane, goes to the physical traction-free boundary, Γ. For a region adjacent to the traction-free elliptical edge in Figs. 1 through 3, the following function maps the region R_ζ of the ζ -plane into region R_z of the z -physical plane where Γ_ζ is a section of the real axis of the ζ -plane, Fig. 5.

$$z = \omega(\zeta) = \frac{a+b}{2}\left(\frac{i-\zeta}{i+\zeta}\right) + \frac{a-b}{2}\left(\frac{i+\zeta}{i-\zeta}\right) + z_c \tag{34}$$

Quantities a and b are the lengths of the major (parallel to the horizontal x -direction) and minor (parallel to the vertical y -direction) axes of the ellipse, respectively, and z_c is the center of the ellipse, Figs. 1 and 5. For convenience, the origin of the coordinate system is chosen at the center of the ellipse, i.e., $z_c = 0$. Substituting equation (34) into $z_j = x + \mu_j y$ produces

$$z_j = \omega_j(\zeta_j) = \frac{a - ib\mu_j}{2}\left(\frac{i-\zeta_j}{i+\zeta_j}\right) + \frac{a+ib\mu_j}{2}\left(\frac{i+\zeta_j}{i-\zeta_j}\right), \quad j = 1,2 \tag{35}$$

The derivatives of this mapping function are

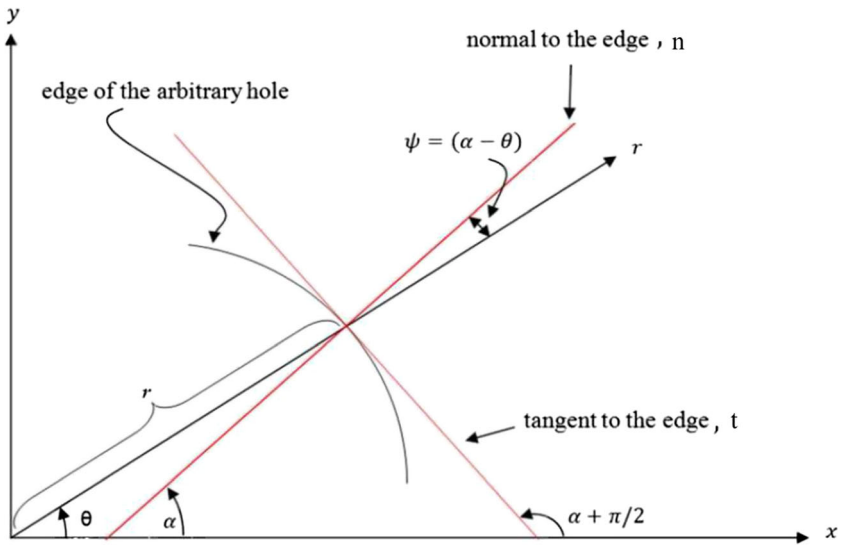

Fig. 4 Coordinate systems

$$\omega_j'(\zeta_j) = -i\frac{a-ib\mu_j}{(i+\zeta_j)^2} + i\frac{a+ib\mu_j}{(i-\zeta_j)^2}, \quad j=1,2 \tag{36}$$

and the inverse of the induced mapping functions are

$$\zeta_j = \omega_j^{-1}(z_j) = i\frac{a-ib\mu_j - \left(z_j \pm \sqrt{z_j^2 - a^2 - b^2\mu_j^2}\right)}{a-ib\mu_j + \left(z_j \pm \sqrt{z_j^2 - a^2 - b^2\mu_j^2}\right)}, \quad j=1,2 \tag{37}$$

The branch of the square root in equation (37) is chosen such that $Im\ \zeta_j \leq 0$ for $j=1,2$.

For a region adjacent to an elliptical hole of major radius, a, and minor radius, b, the following function using $z_j = x + \mu_j y$ where $x = a\cos\theta$ and $y = -b\sin\theta$

$$z_j = \omega_j(\zeta_j) = \frac{a-ib\mu_j}{2}\frac{1}{\zeta_j} + \frac{a+ib\mu_j}{2}\zeta_j, \quad j=1,2 \tag{38}$$

maps the region of a unit circle, R_ζ, in the ζ -plane into the region R_z in the z -physical plane. The derivatives of this mapping functions are

$$\omega_j'(\zeta_j) = \frac{a+ib\mu_j}{2} - \frac{a-ib\mu_j}{2}\frac{1}{\zeta_j^2}, \quad j=1,2 \tag{39}$$

and the inverse of the induced mapping functions are

$$\zeta_j = \omega_j^{-1}(z_j) = \frac{z_j \pm \sqrt{z_j^2 - a^2 - \mu_j^2 b^2}}{a+ib\mu_j}, \quad j=1,2 \tag{40}$$

The branch of the square root in equation (40) is chosen such that $|\zeta_j| < 1$ for $j=1,2$.

Finite Element Analysis

For comparison with the TSA results, a finite element analysis (FEA) using ANSYS prediction was prepared of the plate of Fig. 1 and the elastic properties of Table 1. Due to the symmetry, only the upper right quarter of the plate was modeled with symmetrical boundary conditions applied at the bottom and left edges. Based on the static equivalent, a far-field stress of

$$\sigma_0 = \frac{F}{A} = 17.68\ MPa\ (2,564\ \text{psi})$$

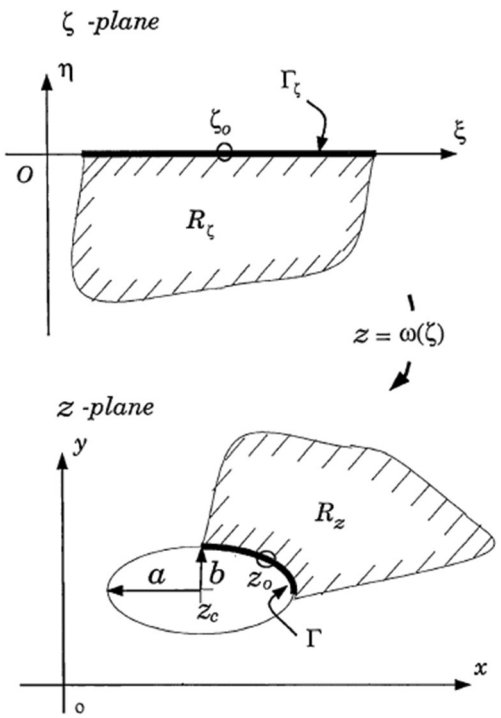

Fig. 5 Conformal mapping for elliptical boundary

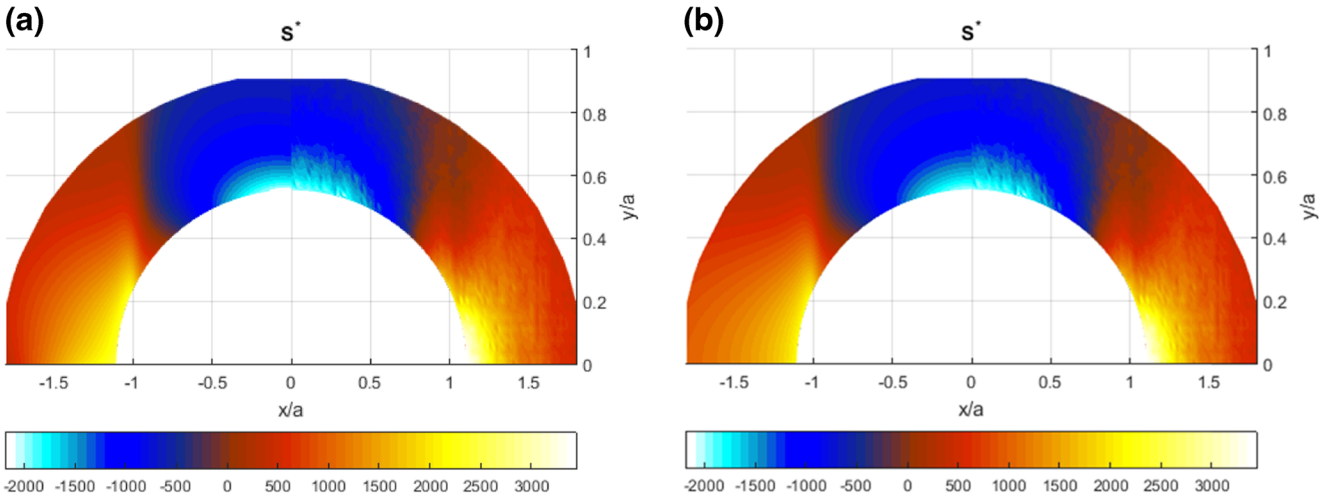

Fig. 6 Contour plots of recorded (*right*) and reconstructed (*left*) *S** throughout region adjacent to elliptical hole using (**a**) Taylor and (**b**) Laurent series expansion (4 complex coefficients)

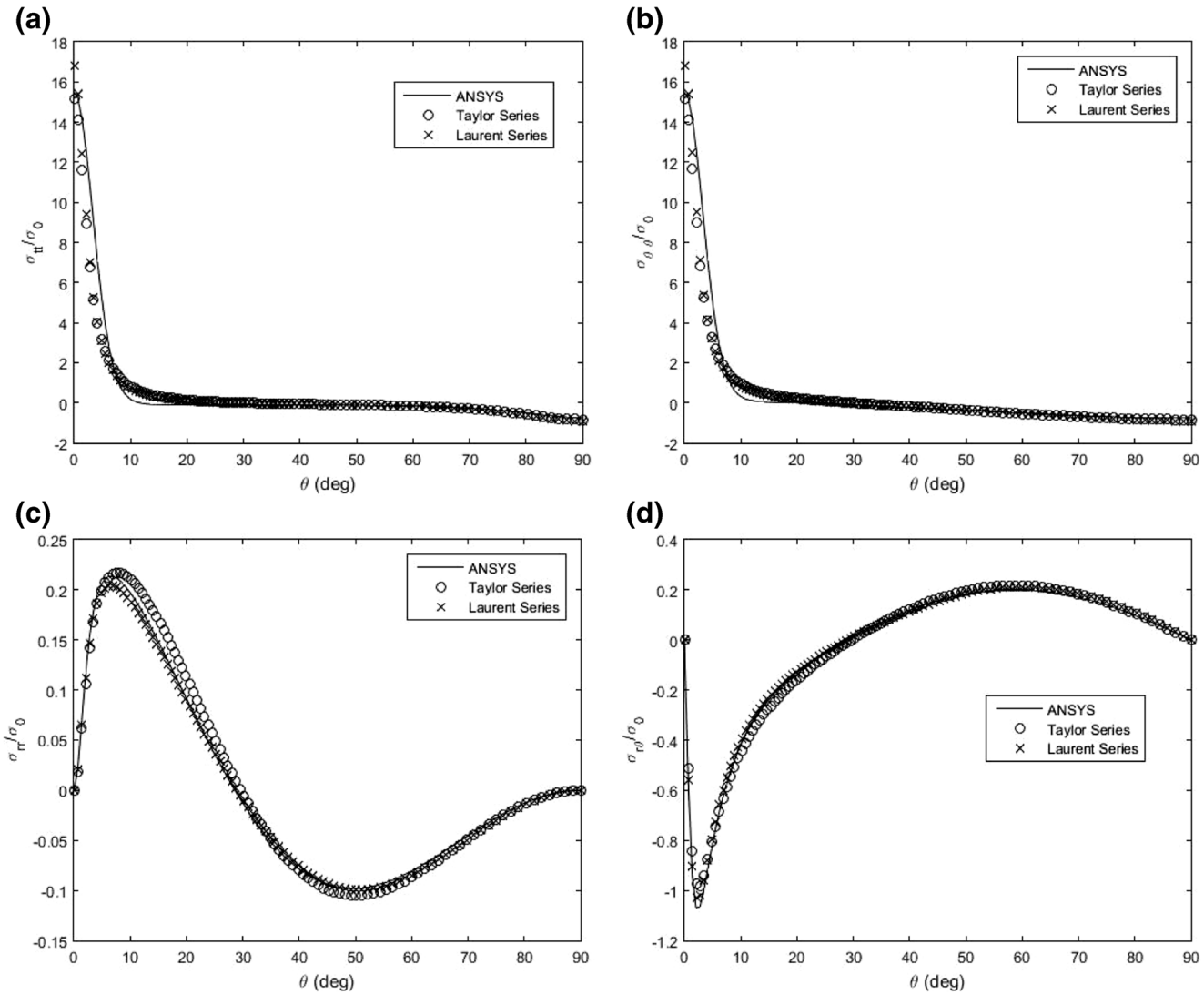

Fig. 7 Plots of (**a**) σ_{tt}/σ_0, (**b**) $\sigma_{\theta\theta}/\sigma_0$, (**c**) σ_{rr}/σ_0 and (**d**) $\sigma_{r\theta}/\sigma_0$ along edge of hole from ANSYS and TSA (Taylor and Laurent series)

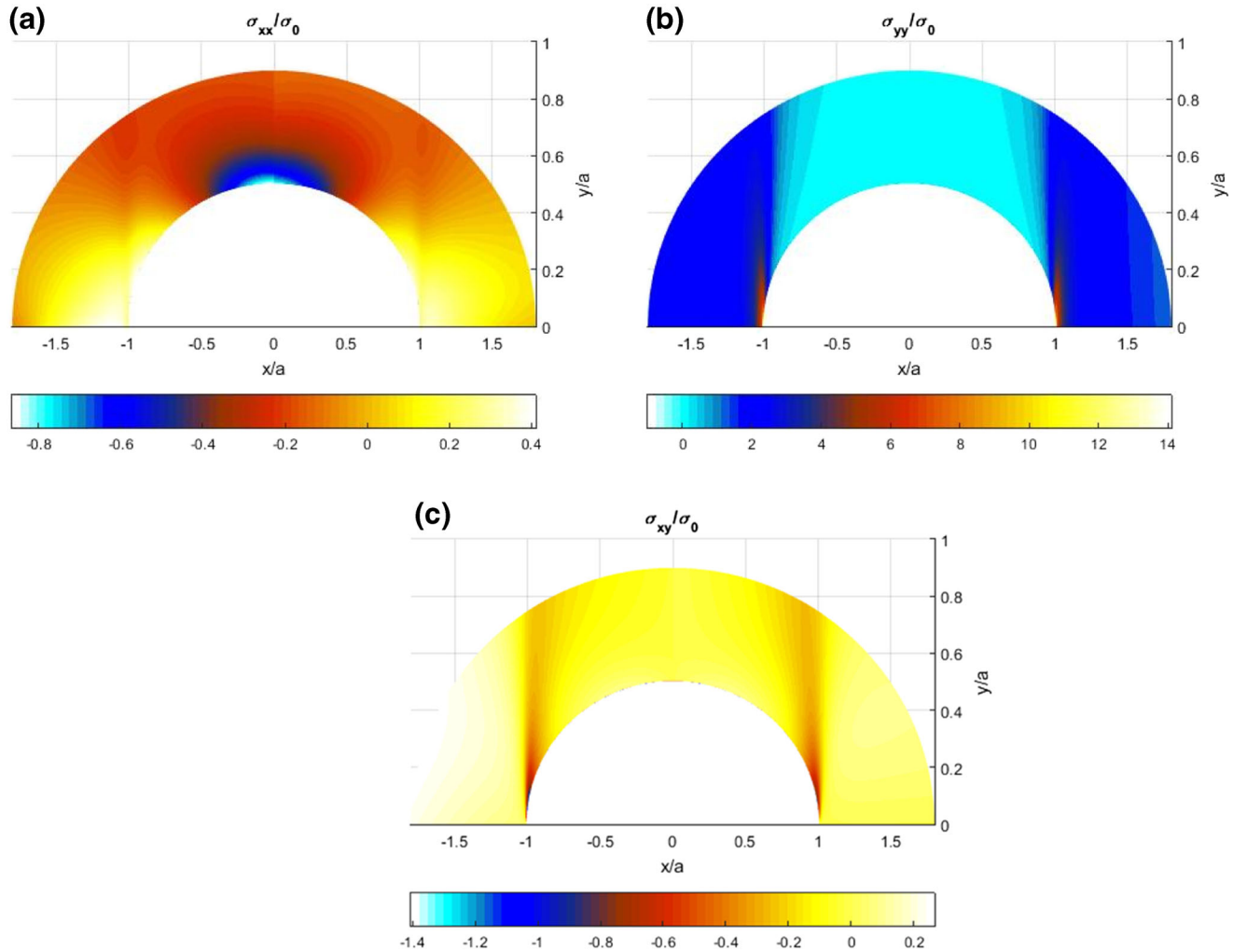

Fig. 8 Contours plot of (**a**) σ_{xx}/σ_0, (**b**) σ_{yy}/σ_0, and (**c**) σ_{xy}/σ_0 throughout region adjacent to hole by FEA (right) and (right) TSA using Taylor series

was applied numerically to the top edge of the plate. Plane 82 Isoparametric elements with eight nodes were employed. Very small elements were used in the neighborhood of the elliptical hole to obtain reliable data. A convergence test was applied until the change in results of the maximum stress between two successive meshing was less than 2 %. The FE model utilizes 67,500 elements and 68,101 nodes. A motivation for developing the present ability is to enable stress analysis of orthotropic cases experimentally which cannot be analyzed numerically, although FEM is used here. The geometry and loading of the Fig. 1 were deliberately selected so as one could obtain a reliable FEA result with which to validate the experimental results. The developed TSA method is applicable to more complicated problems which are difficult for FEM. For example, while industry makes prevalent use of FEM, strain gages are often employed in that environment to obtain the boundary conditions for the FEA.

Results

The complex coefficients, $A_j = a_j + ib_j$, were evaluated by two approaches: the first approach uses equations (35) through (37) and the Taylor representation of the stress function of equation (18) to map the physical plane to a half-plane in ζ-plane; the second approach uses equations (38) through (40) and the Laurent series expansion of equation (19) to map the physical plane to the unit circle in the ζ-plane. The unreliable thermoelastic data on and near the elliptical boundary motivated using only thermoelastic data from 1.1 a and 1.1 b to 1.85 a and 1.85 b. The complex coefficients A_j were evaluated individually from equations (28) or (29) employing the recorded thermoelastic data inside the region, R^*, utilizing the Taylor and Laurent representations for the stress function, respectively. The individual stresses throughout region R_z, including on the edge Γ where no thermoelastic input data were employed, were evaluated using equations (22) through (24) for the Taylor expansion or equations (25) through (27) for the

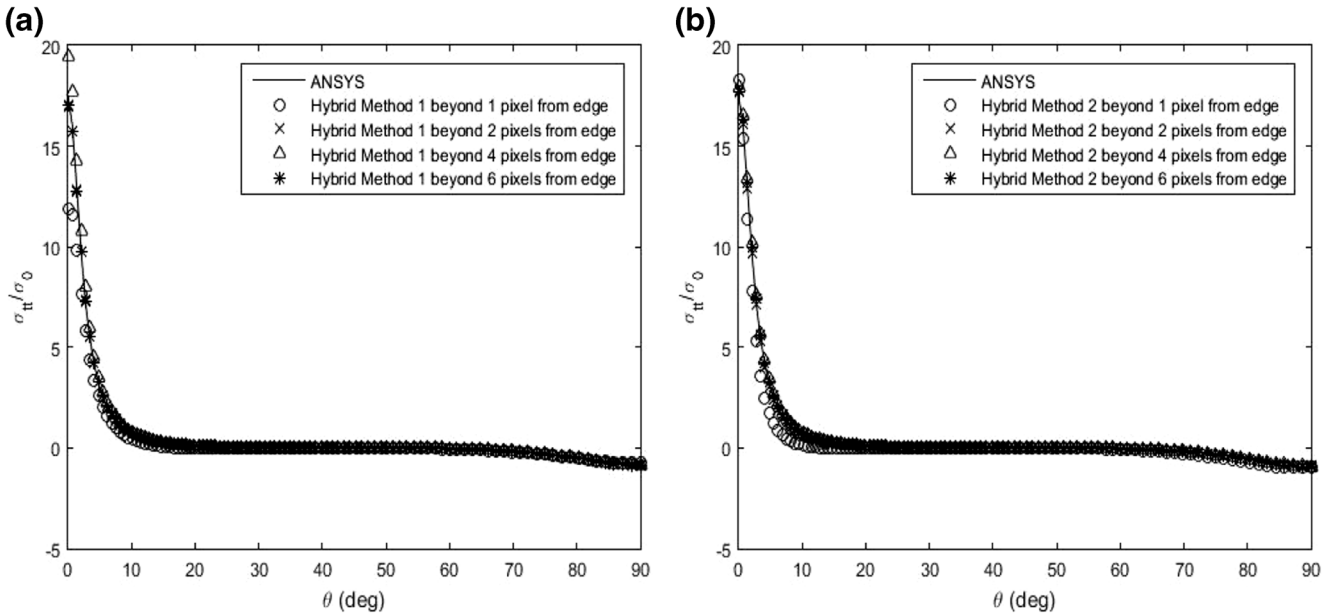

Fig. 9 Effect of pixel location on TSA-determined σ_{tt}/σ_0 along edge of hole using (**a**) Taylor series, (**b**) Laurent series

Laurent expansion. Among other techniques, the number of complex Airy coefficients, N, to retain in the stress functions was assessed by evaluating the difference between the magnitude of experimentally based thermoelastic data and those predicted by the present hybrid method using the root mean square (RMS) method. This RMS analyses and the condition number of Airy matrix suggests using 8 real coefficients is suitable with either the first (Taylor expansion) and second (Laurent expansion) approach. Having determined how many Airy coefficients to retain, their values were determined by least squares. Knowing the magnitudes of the Airy coefficients, the stresses are available from equations (22) through (27). The appropriateness of utilizing $N=4$ complex coefficients is substantiated by comparing the reconstructed and experimentally-based, S^*, Fig. 6. The tangential stress, σ_{tt}, from equation (33) and the polar components of stress from equations (30), normalized with respect to σ_0 = 17.68 MPa, are plotted on the edge of the hole in Fig. 7. Not surprising, the magnitudes of σ_{tt}/σ_0 and $\sigma_{\theta\theta}/\sigma_0$ are very similar to each other, and $\sigma_{r\theta}/\sigma_0$ and $\sigma_{r\theta}/\sigma_0$ are small, on the edges of the hole. Contour plots of normalized Cartesian components of stress by the hybrid technique using the first approach (Taylor series) and ANSYS are plotted in Fig. 8. These TSA-based results agree with FEM predictions.

TSA reliability was further assessed by checking load equilibrium. This was done by numerically integrating the TSA-determined vertical stress, σ_{yy}, along the line $y = 0$ (line AB in Fig. 1),

$$F = \int \sigma_{yy} dA = 2 \int_a^{W/2} \sigma_{yy} t dx$$

where t and W are the plate thickness and width, respectively. The integration of the TSA-determined stress was computed using the trapezoidal rule. Results based on the Taylor and Laurent representations are 7.4 kN (1658 lb) and 6.8 kN (1529 lb), respectively, both of which are close to the physically applied load of 7.12kN (1600 lbs.).

Effect of Input Data Location

Since recorded TSA data at and close to an edge are unreliable, one typically does not employ measured data within two or three pixels away from the edge of the hole. The previous results are based here on the 2558 recorded values of S^*, all of which originate 6 pixels (0.1 a = 2 mm) away from the edge of the hole. A small subroutine was subsequently prepared to assess the effect on the tangential stress, σ_{tt}, at the edge of the hole when employing S^* data at different minimum distances (number of pixels) from the hole, Fig. 9. These results demonstrate that neither the Taylor nor Laurent formulations are acceptable with thermal information collected up to one pixel away from the edge of the hole. Rather, one should use TSA data which originates at least 2 pixels away from the edge of the hole.

Summary, Discussion and Conclusions

A hybrid method which processes the load-induced TSA signals with a stress function in complex variables, together with conformal mapping and analytic continuation

concepts, provides the individual stresses on and in the neighborhood of an elliptical hole in a finite orthotropic composite plate. Both Laurent and Taylor series representations of the stress function are utilized with equal satisfaction. Unlike purely theoretical or numerical methods, knowledge of the external boundary conditions is unnecessary. TSA results agree with those from FEM and force equilibrium. Results demonstrate the need to not employ recorded TSA data within at least two pixels of the edge of the hole. Unlike previous TSA approaches, rational means are provided with which to assess how many coefficients to retain and the suitability of employing either the Laurent or Taylor series representation is shown experimentally. More complicated shaped cutouts might necessitate the use of overlapping applications of the method.

A motivation for developing the present method is to enable stress analysis of orthotropic cases which cannot be analyzed numerically. The present geometry and loading were deliberately selected so as one could obtain a reliable FEA with which to compare the experimental results and thereby validate the presented experimental technique. The developed thermoelastic method is applicable to more complicated problems which are difficult for FEM.

Acknowledgments Abdullah Alshaya was funded by a graduate scholarship from the University of Kuwait.

References

1. Stanley P, Chan WK (1987) The application of thermoelastic stress analysis to composite materials. SEM Spring Conf Exp Mech 536–544
2. Kageyama K, Ueki K, Kikuchi M (1987) Applications of thermoelastic stress analysis to FRP. Presented 32nd National Conf FRP, Tokyo 52–57
3. Kageyama K, Ueki K, Kikuchi M (1998) Thermoelastic technique applied to stress analysis of carbon fiber composite materials. Proc 6th Int Cong Exper Mech 931–936
4. Wong AK (1990) A non-adiabatic theory and use of SPATE on composite laminates. Int'l Cong Exper Mech, Copenhagen
5. Feng Z, Zhang D, Rowlands RE, Sandor BI (1992) Thermoelastic determination of the individual stresses in loaded composites. Exp Mech 32(2):89–95
6. Lin ST, Rowlands RE (1995) Thermoelastic stress analysis of orthotropic composites. Exp Mech 35(3):257–265
7. Khaja AA, Rowlands RE (2015) Experimentally determined stresses associated with elliptical holes using polar Coordinates. Strain 49(2):116–124
8. Samad WA, Rowlands RE (2013) Full-field thermoelastic stress analysis of an unsymmetrically-loaded elliptically-perforated Structure". Photomechanics2013, Montpellier, France
9. Private communication (PhD Prelim document, 2016)) with Narin Fatima, University of Wisconsin-Madison, Madison, WI, USA
10. Lekhniskii SG (1956) Anisotropic plates. Gordon & Breach Scientific Publishers, New York
11. Bowie OL, Freese CE (1972) Central crack in plane orthotropic rectangular sheet. Int J Fracture Mech 8(1):49–57
12. Gerhardt TD (1984) A hybrid finite element approach for stress analysis of notched anisotropic materials. J Appl Mech 15(4): 804–810
13. Khaja AA (2012) Experimentally determined full-field stress, strain and displacement analysis of perforated finite members, PhD Thesis, University of Wisconsin-Madison, Madison, WI